CrystEngComm

Dynamic Article Links

Cite this: *CrystEngComm*, 2011, **13**, 3900

www.rsc.org/crystengcomm

PAPER

$CaCu_3Ti_4O_{12}$ single crystals: insights on growth and nanoscopic investigation

Patrick Fiorenza,[a] Vito Raineri,[a] Stefan G. Ebbinghaus[b] and Raffaella Lo Nigro*[a]

Received 14th December 2010, Accepted 17th March 2011
DOI: 10.1039/c0ce00948b

The combination of scanning impedance microscopy and conductive atomic force microscopy was applied to single crystals of the perovskite-type oxide $CaCu_3Ti_4O_{12}$ (CCTO) in order to provide a local dielectric characterization on ingot sections. Both techniques clearly showed dielectric heterogeneities due to the presence of inclusions within crystals grown in different laboratories. Despite macroscopic characterizations, such as Laue diffraction, gave no indications for the presence of inclusions within the crystals, the discovery of dielectric heterogeneities prompted a careful structural analysis, which revealed the presence of crystalline $CaTiO_3$ (CTO) precipitates. Thus, the scanning probe investigation provided the evidence for the electrical homogeneity within the CCTO crystal and the presence of internal barriers due to the CCTO/CTO interfaces.

Introduction

The complete investigation of single crystals certainly represents the most valid method for understanding the intrinsic properties of complex oxide materials. In fact, the physical and chemical properties of functional materials, such as perovskite oxides, might be strongly affected by the presence of bulk defects and/or of different compositions at the grain boundaries favouring extrinsic properties at nanoscale. Among the perovskite-type oxides, calcium copper titanate $CaCu_3Ti_4O_{12}$ (CCTO)[1] has attracted considerable attention in recent years due to its impressive permittivity value of $\sim 10^4$ to 10^5 at 1 MHz, which remains constant in the 100–600 K temperature range.[2–17] This "giant" permittivity has been observed in both CCTO single crystals[2–9] and ceramics,[10–17] while in CCTO thin films[18–20] permittivities are one order of magnitude lower. Several interpretations of this "giant" phenomenon have been proposed. For instance, impedance spectroscopy has revealed CCTO ceramics to be electrically heterogeneous and to consist of semiconducting grains and insulating grain boundaries. In this case, the giant permittivity effect has been explained using the well-known Internal-Barrier-Layer-Capacitor (IBLC) model.[10–13,17] Although this model works reasonably well for CCTO ceramics, the observation of the giant permittivity effect in CCTO single crystals remains perplexing as grain boundaries should not be present. The origin of the effect in single crystals may therefore be related to different phenomena, not observed in the ceramics, *e.g.* non-ohmic contact (Surface-Barrier-Layer-Capacitor (SBLC) effect), modification of crystal surface composition and/or internal boundary layers associated with defects, twins, dislocations, *etc.*[3–9] In this context, it seems that the origin of giant permittivity in CCTO ceramics and crystals should be different: the CCTO single crystal behaviour can be well interpreted by SBLC effects associated to a non-ohmic electrode contact, while the IBCL effect works quite well for CCTO ceramics, but the non-ohmic electrode effect can be present if the resistance at the grain boundaries is <100 kΩ cm.[17]

On the other hand, it should be noted that the IBLC model for the CCTO ceramics has been corroborated by nanoscopic investigations carried out with different scanning probe microscopy techniques (Conductive-Atomic Force Microscopy (C-AFM), Scanning Impedance Microscopy (SIM) and Kelvin probe force microscopy).[14,21–23] Nanoscopic investigation on CCTO ceramics imaged and demonstrated the electrical properties of the grain boundaries. They are clearly insulating and the thickness of the depletion layer at the grain–boundary interfaces has been determined to be about 100 nm.[21–23] Analogous nanoscopic investigation has never been reported for CCTO single crystals, despite it could be very important to study and compare the structural, chemical and dielectric properties of single crystals after deep investigations by both micro- and nano-methodologies.

This paper reports on the use of Scanning Probe Microscopy (SPM) based techniques to study dielectric characteristics within CCTO single crystals. In particular, appealing data have been obtained by SIM and C-AFM measurements performed on CCTO single crystals, which appeared to be pure materials by conventional Laue diffraction characterization. Electrical homogeneity within the CCTO crystals has been found, but also the presence of insulating inclusions not deducted by all the macroscopic techniques used for their structural, compositional and electrical characterization. The investigation on nanoscale

[a]*Istituto per la Microelettronica e Microsistemi (IMM), Consiglio Nazionale delle Ricerche (CNR), Strada VIII 5, 95121 Catania, Italy. E-mail: raffaella.lonigro@imm.cnr.it; Fax: +39 095 5968312; Tel: +39 095 5968218*

[b]*Institut für Chemie, Martin-Luther-Universität Halle-Wittenberg, Kurt-Mothes-Str. 2, 06120 Halle, Saale, Germany*

by the C-AFM and SIM techniques provided not only electrical information but also pointed out to structural and compositional heterogeneities not detectable by conventional micro-characterization techniques. The imaging electrical homogeneity represents an important issue for the evaluation of the giant dielectric response in CCTO single crystals.

Results and discussion

$CaCu_3Ti_4O_{12}$ (CCTO) single crystal preparation and structural characterization

CCTO single crystals have been prepared by the travelling solvent floating zone method. The picture of a CCTO circular slice from the original cylindrical crystal is reported in Fig. 1a. Before the scanning probe microscopy investigations, the surface of CCTO crystals has been polished in order to avoid artefacts during measurements due to roughness and/or any possible superficial contamination/impurities. The low magnification Scanning Electron Microscopy (SEM) image shows the polished part of the CCTO crystal (area inside the white square in Fig. 1a) which is clearly visible in the magnification on Fig. 1b.

The structural characterization has been performed by Laue diffraction measurements. In particular, Fig. 2 shows a Laue backscattering image of the CCTO crystal recorded with copper radiation. Overlayed is the simulation, which reveals the single crystalline character of the sample. The orientation of the surface was almost parallel to the {100} direction of the cubic cell with a misorientation $<1.5°$ 2θ. No other features different from CCTO phase are present. Thus, on the basis of the Laue diffraction analysis, the CCTO single crystal is pure and {100} oriented.

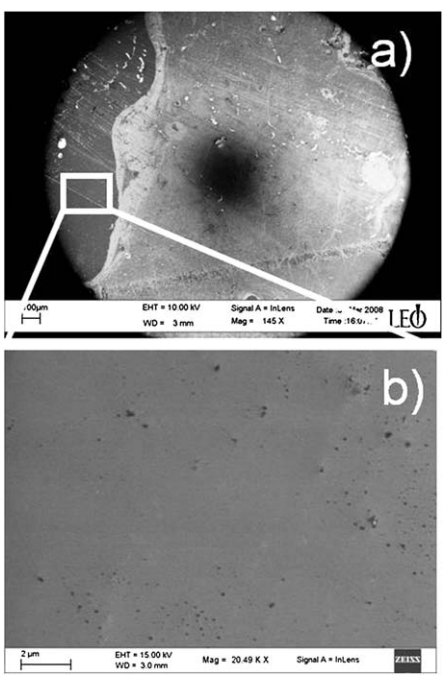

Fig. 1 (a) SEM image at low magnification of CCTO crystal showing the polished part of the sample and (b) magnification of the polished part.

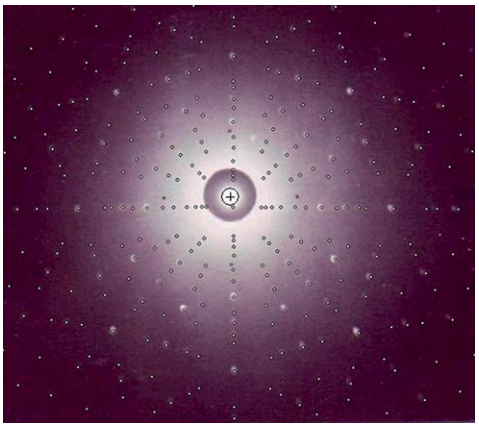

Fig. 2 Laue back scattering diffraction indicating that the CCTO sample is a pure and almost (100) oriented single crystal, as demonstrated by the overlay of the simulation.

Dielectric characterization

Dielectric characterization has been already reported for the CCTO single crystal. In the 10^1 to 10^6 Hz frequencies range it showed "giant permittivity" (ε' up to 10^5),[4,5,8,17] while at higher frequencies in the GHz region the ε' values decrease to about 200–100. The origin for such behaviour has been widely discussed.[4–9]

Moreover, a comprehensive study carried out by impedance spectroscopy (IS) upon varying the chemical nature of the electrode contacts (*i.e.* Au and InGa) demonstrated the presence of two R_1C_1 and R_2C_2 elements (RC = resistor–capacitance) to the permittivity.[17] The R_1C_1 element does not depend on the chemical nature of the electrode and it represents the contribution of the bulk (ε intrinsic value $\sim$100). By contrast, the R_2C_2 element depends on the electrode material, thus providing evidence for the formation of a Schottky barrier due to the non-ohmic contact at the CCTO/electrode interface. All the IS data on CCTO single crystals have been compared to those obtained from CCTO ceramics and on the basis of the relative complex impedance (Z^*) curve shape and of R_2 values: it has been argued that the electrode effect is the main reason for the occurrence of giant permittivity in CCTO single crystal.

On the other hand, the IS studies cannot provide any information on the possible presence of defects and insulating heterogeneities in CCTO crystals (having a semiconductor nature), and they cannot reveal their influence on the measured physical properties. In this context, nanoscopic techniques have to be employed to clarify this aspect of the crystal investigation.

Scanning Probe Microscopy on $CaCu_3Ti_4O_{12}$ crystals

The Scanning Probe Microscopy (SPM) represents the general definition of a number of techniques useful for the direct imaging of micro- or nano-structures[24–26] and for the identification of dielectric heterogeneities.[27–29] These techniques provide information (with high lateral resolution) on the local conduction and insulating regions because of the conductive AFM tip which, moving over the sample surface, acts as a sliding metal contact: by applying a bias between the bottom electrode and the tip, it is possible to collect the current (C-AFM) or the impedance signal

(SIM) of the nano-devices.[26,27] Here both C-AFM and SIM techniques have been applied for a deep investigation of the giant dielectric constant phenomenon in CCTO crystals.

SPM investigations have been performed on CCTO single crystals after polishing treatments and fabrication of a silver paste bottom electrode, while the top electrode is represented by the AFM tip.

In Fig. 3 the SPM images of the CCTO crystal are given. The morphological images (Fig. 3a and c) show a flat crystal (the root mean square, calculated on $50 \times 50\ \mu m^2$ area, is about 1 nm). By contrast, the SIM and C-AFM maps (Fig. 3b and d) revealed the presence of an inclusion, which is darker than the CCTO bulk indicating that it is more insulating.

Further dielectric investigations have been carried out by stopping the C-AFM tip and ramping the applied dc bias on both the inclusion and the bulk. The recorded *I–V* curves (Fig. 4a) pointed to a possible blocking effect caused by the inclusions. In fact, as shown in Fig. 4a, the current flowing through the inclusion (red experimental points) is one order of magnitude lower than in the CCTO matrix (blue solid circles).

Stopping the tip motion, in SIM mode, it was also possible to collect the d*C*/d*V versus* voltage curves, as shown in Fig. 4b. The d*C*/d*V* curve acquired on CCTO single crystal (Fig. 4b, blue solid circles) shows a single peak, while the curve acquired on the inclusion (Fig. 4b, red open squares) presents two peaks. By integration of the experimental curves, the relative capacitance *versus* voltage curves have been obtained (Fig. 4c). A step-like behaviour typical of an ideal Metal–Insulator–Semiconductor device (where the semiconductor is n-type) has been observed in the CCTO single crystal, while in the inclusions a double step behaviour has been found.

Moreover, analogous SIM and C-AFM characterizations have been performed on a second CCTO single crystal (in the following indicated as CCTO1), grown in a different laboratory. The provided CCTO1 crystal (Fig. 5a) yielded similar results. In this case also the morphological images (Fig. 5b and d) show an inclusion within the crystal. The squared inclusion size is about $10 \times 10\ \mu m^2$. The inclusion dielectric behaviour has been clarified by SIM (Fig. 5c) and C-AFM (Fig. 5e) investigations: it is, like in our CCTO sample, more insulating than the crystal bulk.

The presence of crystalline inclusions, discovered by the nanoscale investigation on two different CCTO crystals, prompted a deeper and more accurate structural/chemical analysis.

The structural/chemical nature of the insulating inclusions within the CCTO crystals has been evaluated by Transmission Electron Microscopy (TEM). Fig. 6a shows a TEM micrograph of the CCTO single crystal. It is clearly visible a well-crystalline inclusion, about 5 μm wide, having a lighter contrast within the CCTO crystal. The selected area electron diffraction pattern (Fig. 6b) obtained from the inclusion can be identified as the

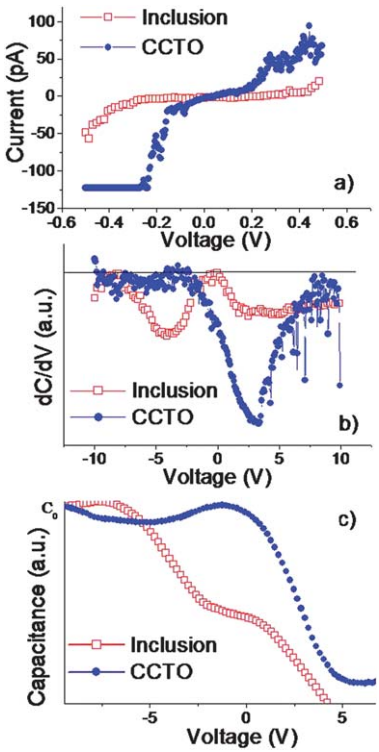

Fig. 4 (a) The *I–V* curves, collected with the C-AFM on both the CCTO bulk (solid circle curve) and insulating inclusion (open square curve), clearly demonstrated the insulating nature of the inclusion with respect to the bulk; (b) d*C*/d*V vs.* voltage curves both on the CCTO bulk (solid circle curve) and within the insulating inclusion (open square curve) have been obtained by stopping the AFM tip on single point and changing the voltage. One peak has been obtained on CCTO bulk, while two peaks are present in the d*C*/d*V* curve from the inclusion; (c) the integrated capacitance *vs.* voltage curves obtained from the experimental d*C*/d*V*.

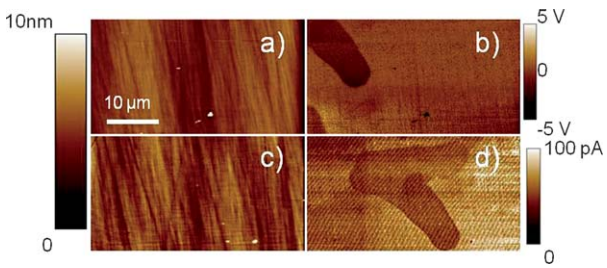

Fig. 3 SPM images performed on CCTO single crystal: (a and c) the AFM morphologies, collected in contact mode, do not show any features; (b) impedance and (d) current maps.

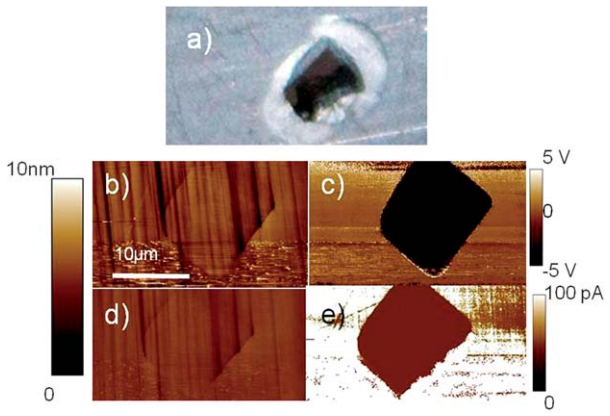

Fig. 5 (a) Picture of the CCTO1 crystal and its SPM images: (b and d) AFM morphologies obtained in contact mode; (c) impedance and (e) current maps.

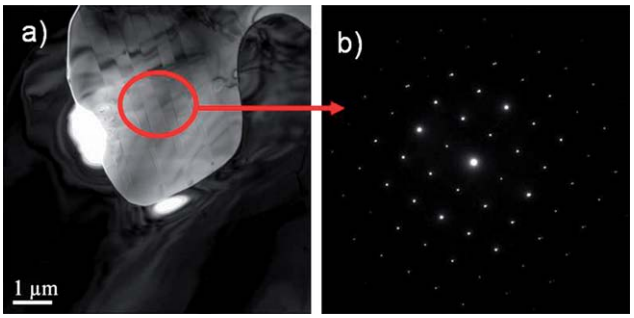

Fig. 6 (a) TEM plan view image of the CCTO crystal and (b) selected area electron diffraction (SAED) of the inclusion visible in (a). The SAED pattern indicates that the inclusion phase is $CaTiO_3$.

(001) plane of the orthorhombic cell of calcium titanate ($CaTiO_3$). Most of the $CaTiO_3$ (CTO) inclusions are perfectly oriented with respect to the CCTO single crystal, *i.e.* the [001] CTO//[001] CCTO, and some of them showed a different orientation parallel to the [001] CCTO.

We also tried to estimate the number of CTO inclusions per unit volume from the current and impedance maps and it has been found to be >1%. In particular, the map areas (corresponding to the crystal investigated area) are 100 μm^2 and since the CTO inclusions are almost insulating, the electrical signal can be collected from a sample thickness of about 10 μm. Thus, the investigated total crystal volume is 10^5 μm^3. Almost one inclusion (having a volume size not bigger than 10^3 μm) has been found for each investigated area, so it is possible to conclude that the CTO/CCTO volume ratio is about 1/100.

These inclusions have not been detected by the macroscopic Laue diffraction for the following possible reasons: (i) firstly, the relatively small fraction of the secondary phase leads to only very low intensities on the photograph, which may not be visible to the eye; (ii) secondly, it is possible that the X-ray spot (roughly 1 mm in diameter) simply "missed" the inclusions although several different points on the crystal (both front and backside) were investigated. In addition, the penetration depth of the X-ray beam is limited, making inclusions underneath the surface undetectable. Finally, the (averaged) unit cell parameter of the identified phase $CaTiO_3$ is almost 1/2 of the unit cell parameter of CCTO, so the diffraction spots overlap in the case of a topotactical growth of both components.

Thus, the presence of insulating CTO inclusions causes the electrical heterogeneities within CCTO single crystals.

The CCTO/CTO system deserves some attention since it can be represented as a heterojunction shown in Fig. 7. The present heterojunction between the CCTO crystal and the CTO inclusion shows a pin in the valence band due to both the n-type semiconductivity of the CCTO and the insulating nature of the CTO, and secondly due to the CTO larger band gap compared to CCTO. Several works demonstrated a similar behaviour in more conventional systems such as Si or Si–Ge structure.[30,31]

In summary, the present scanning probe characterization provides two important information not available with the previous macroscopic measurements:

- it seems to be extremely hard to grow pure CCTO single crystals, in fact, both the investigated CCTO crystals possess inclusions. On the other hand, it has been demonstrated by thermogravimetric analysis that CCTO ceramics easily reduce to $CaTiO_3$, TiO_2 and Cu,[32] thus also in the synthesis process the formation of one of these phases might occurred.

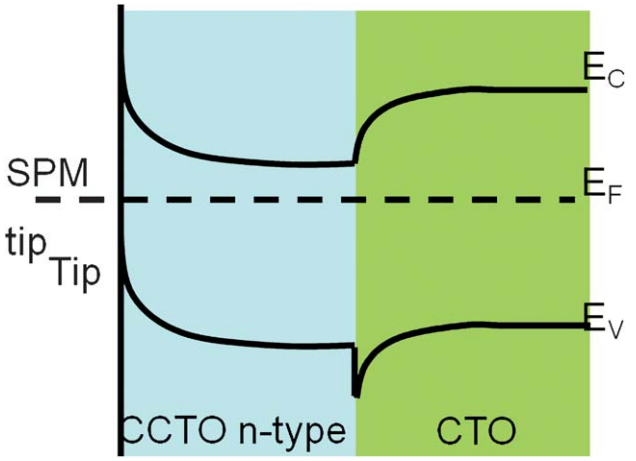

Fig. 7 Band diagram scheme representing the heterostructure formed at the insulating inclusion/CCTO crystal interface. The present heterojunction shows a pin in the valence band due to both the n-type semiconductivity of the CCTO and the insulating nature of the CTO and secondly due to the CTO larger band gap compared to CCTO.

- the interpretation of macroelectrical analysis might induce to incomplete conclusions because they did not provide experimental evidence of insulating inclusions.

Recently, also in the case of CCTO ceramics, great attention has been devoted to the role of nanosized internal insulating barrier layers due to staking faults or nanodomains originating within grains.[33–35] Some works, in fact, described the presence of defects such as stacking faults and/or nanodomains within the grains of CCTO ceramics and they support the idea that the internal barrier layer capacitance (IBCL) mechanism is enhanced by another similar effect, operating in the nanoscale range, referred to as "nanoscale barrier layer capacitance model (NBCL)".[33–35] On the basis of this argumentation, the presence of $CaTiO_3$ precipitates may affect the conduction mechanisms in CCTO single crystal and because of their different electrical conductivity could contribute to explain the CCTO single crystal electric response. The aim of the NBCL model is to provide a common explanation/origin of giant permittivity for CCTO in all its forms (crystals and polycrystalline ceramics). Certainly it is no trivial to isolate the nanoscale barrier layer contributions, but to date no nanoscopic investigation has been reported for CCTO crystals and no direct evidence for internal barrier layer has been provided.

Conclusions

C-AFM and SIM investigations demonstrated the presence of insulating inclusions in $CaCu_3Ti_4O_{12}$ single crystals grown in different laboratories. The presence of these inclusions has not been previously observed by macroscopic techniques used for the structural, compositional and electrical characterization. TEM analyses have been performed and the insulating inclusions have been identified to be $CaTiO_3$. The $CaTiO_3$ secondary phase could

block/restrict conduction within $CaCu_3Ti_4O_{12}$ crystals and could participate in the macroscopic conduction mechanisms.

It is noteworthy that the experimental approach presented in this paper could be used to investigate the dielectric properties of a wide class of inhomogeneous materials. In particular experimental proof of the detection of insulating inclusions, embedded in semiconducting matrix, has been provided. This represents a step forward with respect to the standard macroscopic electrical characterization techniques.

Experimental

Single crystal CCTO was grown by the travelling solvent floating zone technique. The applied growth furnace (model GERO SPO) is equipped with two 1000 W halogen lamps, the radiation of which is focused by gold-coated ellipsoidal mirrors. Polycrystalline bars serving as seed and feed rods were cold-pressed and sintered in air for 12 h at 1000 °C. Since CCTO does not grow congruently, the tip of the feed rod was enriched with 20% CuO acting as self-flux. A growth rate of 5 mm h^{-1} was used and the seed rod was rotated with a speed of 30 rpm, while the feed was kept still. To avoid the thermal reduction of copper at the high temperatures required, the crystal growth was performed in pure oxygen with a pressure of 4 bar and a gas flow rate of 0.2 l min^{-1}.

Laue diffraction was performed in reflection geometry with a Huber diffractometer. The distance between the sample and the Polaroid© photo film was 40 mm. White X-ray radiation was generated with a Cu tube (30 kV, 30 mA). The sample was illuminated for 3 minutes.

CCTO single crystals were observed by a Leo Iridium 1450 Scanning Electron Microscope.

The CCTO single crystal slices were polished to eliminate the influence of superficial artefacts in the SPM mapping. Measurements were performed using a back side contact, obtained by silver paint, opposite to the polished surface. Measurements at nanometre scale were performed by a Digital Instrument D3100 atomic force microscope (AFM) with a Nanoscope V controller operating in air and in contact, equipped with the tunnelling atomic force microscopy (TUNA) module. SIM measurements were carried out in constant ΔV mode by a Digital Instruments Dimension 3100 atomic force microscope. The ac bias applied between the tip and sample was varied in the 1–10 V peak-to-peak range at 90 kHz; the resonator frequency was in the range 1.0 ± 0.1 GHz.

The CCTO single crystals were examined by electron microscopy using a field-emission JEOL transmission electron microscope, operating at an accelerating voltage of 200 kV.

Acknowledgements

This work has been supported by European Union under the project NUOTO (New Materials with Ultrahigh *k* dielectric constant fOr TOmorrow wireless electronics) NMP3-CT-2006-032644. S. G. Ebbinghaus acknowledges financial support by the DFG through SFB 484. The authors are also very grateful to Prof. Derek C. Sinclair for providing a $CaCu_3Ti_4O_{12}$ crystal.

References

1 B. Bochu, M. N. Deschizeaux, J. C. Joubert, A. Collomb, J. Chenavas and M. Marezio, *J. Solid State Chem.*, 1979, **29**, 291–298.
2 C. Homes, T. Vogt, S. M. Shapiro, S. Wakimoto and A. P. Ramirez, *Science*, 2001, **293**, 673–676.
3 M. H. Cohen, J. B. Neaton, L. He and D. Vanderbilt, *J. Appl. Phys.*, 2003, **94**, 3299–3306.
4 S. Krohns, P. Lunkenheimer, S. G. Ebbinghaus and A. Loidl, *Appl. Phys. Lett.*, 2007, **91**, 022910.
5 S. Krohns, P. Lunkenheimer, S. G. Ebbinghaus and A. Loidl, *J. Appl. Phys.*, 2008, **103**, 084107.
6 M. A. Subramanian and A. W. Sleight, *Solid State Sci.*, 2002, **4**, 347–351.
7 T. T. Fang and C. P. Liu, *Chem. Mater.*, 2005, **17**, 5167–5171.
8 P. Lunkenheimer, S. Krohns, S. Riegg, S. G. Ebbinghaus, A. Reller and A. Loidl, *Eur. Phys. J. Spec. Top.*, 2010, **180**, 61–89.
9 M. A. Subramanian, D. Li, N. Duan, B. A. Reisner and A. W. Sleight, *J. Solid State Chem.*, 2000, **151**, 323–325.
10 J. Li, A. W. Sleight and M. A. Subramanian, *Solid State Commun.*, 2005, **135**, 260–262.
11 D. C. Sinclair, T. B. Adams, F. D. Morrison and A. R. West, *Appl. Phys. Lett.*, 2002, **80**, 2153–2155.
12 T. B. Adams, D. C. Sinclair and A. R. West, *Phys. Rev. B: Condens. Matter Mater. Phys.*, 2006, **73**.
13 T. B. Adams, D. C. Sinclair and A. R. West, *Adv. Mater.*, 2002, **14**, 1321–1323.
14 S.-Y. Chung, I.-D. Kim and S.-J. L. Kang, *Nat. Mater.*, 2004, **3**, 774–778.
15 W. Li and R. W. Schwartz, *Appl. Phys. Lett.*, 2006, **89**, 242906.
16 J. Li, M. A. Subramanian, H. D. Rosenfeld, C. Y. Jones, B. H. Toby and A. W. Sleight, *Chem. Mater.*, 2004, **16**, 5223–5225.
17 M. C. Ferrarelli, D. C. Sinclair, A. R. West, H. A. Dabkowska, A. Dabkowski and G. M. Luke, *J. Mater. Chem.*, 2009, **19**, 5916–5919.
18 R. Lo Nigro, G. Malandrino, R. G. Toro, M. Losurdo, G. Bruno and I. L. Fragalá, *J. Am. Chem. Soc.*, 2005, **127**, 13772–13773.
19 R. Lo Nigro, R. G. Toro, G. Malandrino, I. L. Fragala', M. Losurdo, M. M. Giangregorio, G. Bruno, V. Raineri and P. Fiorenza, *J. Phys. Chem. B*, 2006, **110**, 17460–17467.
20 G. Deng, T. Yamada and P. Muralt, *Appl. Phys. Lett.*, 2007, **91**, 202903.
21 P. Fiorenza, R. Lo Nigro, C. Bongiorno, V. Raineri, M. C. Ferarrelli, D. C. Sinclair and A. R. West, *Appl. Phys. Lett.*, 2008, **92**, 182907.
22 P. Fiorenza, R. Lo Nigro, V. Raineri, R. G. Toro and M. R. Catalano, *J. Appl. Phys.*, 2007, **102**, 116103.
23 P. Fiorenza, V. Raineri, M. C. Ferrarelli, D. C. Sinclair and R. Lo Nigro, *Nanoscale*, 2011, **3**, 1171–1175.
24 E. Meyer, S. R. Jarvis and N. D. Spencer, *MRS Bull.*, 2011, **29**, 443–448.
25 J. Y. Park, S. Maier, B. Hendriksen and M. Salmeron, *Mater. Today*, 2010, **13**, 38–44.
26 P. Fiorenza, R. Lo Nigro, V. Raineri, S. Lombardo, R. G. Toro, G. Malandrino and I. L. Fragalà, *J. Appl. Phys.*, 2005, **98**, 044312.
27 P. Fiorenza, R. Lo Nigro, V. Raineri, G. Malandrino, R. G. Toro and M. R. Catalano, *J. Appl. Phys.*, 2010, **108**, 074103.
28 Applied Scanning Probe Methods X, in *Nanoscience and Technology Series*, ed. B. Bhushan, H. Fuchs and M. Tomitori, Springer-Verlag, Heidelberg, 2008, ISBN: 978-3-540-74085-8.
29 J. Loos, *Adv. Mater.*, 2005, **17**, 1821–1833.
30 S. Chattopadhyay, K. S. K. Kwa, S. H. Olsen, L. S. Driscoll and A. G. O'Neill, *Semicond. Sci. Technol.*, 2003, **18**, 738–744.
31 S. Maikap, L. K. Bera, S. K. Ray, S. John, S. K. Banerjee and C. K. Maiti, *Solid-State Electron.*, 2000, **44**, 1029–1034.
32 T. B. Adams, D. C. Sinclair and A. R. West, *J. Am. Ceram. Soc.*, 2006, **89**, 3129–2838.
33 P. R. Bueno, R. Tararan, R. Parra, E. Joanni, M. A. Ramirez, W. C. Ribeiro, E. Longo and J. A. Varela, *J. Phys. D: Appl. Phys.*, 2009, **42**, 055404.
34 S. Sarkar, B. K. Chaudhuri and H. D. Yang, *J. Appl. Phys.*, 2010, **108**, 014114.
35 F. Amaral, L. C. Costa, M. A. Valente, A. J. S. Fernandes, N. Franco, E. Alves and F. M. Costa, *Acta Mater.*, 2010, DOI: 10.1016/j.actamat.2010.09.014.

